Mon. Not. R. Astron. Soc. **381,** L30–L34 (2007) doi:10.1111/j.1745-3933.2007.00360.x

Detection of SiO emission from a massive dense cold core

N. Lo,[1,2]★ M. Cunningham,[1] I. Bains,[1,3] M. G. Burton[1] and G. Garay[4]

[1]*School of Physics, University of New South Wales, Sydney, NSW 2052, Australia*
[2]*Australia Telescope National Facility, CSIRO, PO Box 76, Epping, NSW 1710, Australia*
[3]*Centre for Astrophysics and Supercomputing, Swinburne University of Technology, PO Box 218, Hawthorn, VIC 3122, Australia*
[4]*Departamento de Astronomía, Universidad de Chile, Casilla 36-D, Santiago, Chile*

Accepted 2007 July 2. Received 2007 June 26; in original form 2007 May 7

ABSTRACT

We report the detection of the SiO (J = 2−1) transition from the massive cold dense core G333.125−0.562. The core remains undetected at wavelengths shorter than 70 μm and has compact 1.2-mm dust continuum. The SiO emission is localized to the core. The observations are part of a continuing multi-molecular line survey of the giant molecular cloud G333. Other detected molecules in the core include ^{13}CO, C^{18}O, CS, HCO$^+$, HCN, HNC, CH$_3$OH, N$_2$H$^+$, SO, HC$_3$N, NH$_3$, and some of their isotopes. In addition, from NH$_3$ (1,1) and (2,2) inversion lines, we obtain a temperature of 13 K. From fitting to the spectral energy distribution we obtain a colour temperature of 18 K and a gas mass of 2×10^3 M$_\odot$. We have also detected a 22-GHz water maser in the core, together with methanol maser emission, suggesting that the core will host massive star formation. We hypothesize that the SiO emission arises from shocks associated with an outflow in the cold core.

Key words: stars: formation – ISM: jets and outflows – ISM: molecules.

1 INTRODUCTION

1.1 The dense cold core G333.125−0.562

The massive cold dense core G333.125−0.562 ($\alpha_{\mathrm{J2000}} = 16^{\mathrm{h}}21^{\mathrm{m}}35^{\mathrm{s}}$, $\delta_{\mathrm{J2000}} = -50^\circ41'10''$) is located in the G333 giant molecular cloud complex, at a distance of 3.6 kpc. It has a dust mass of 2.3×10^3 M$_\odot$ and an average density of 2×10^5 cm^{-3} (Garay et al. 2004). The cold core was discovered by Garay et al. (2004), comparing the SEST Imaging Bolometre Array (SIMBA) 1.2-mm survey (Faúndez et al. 2004) with *Midcourse Space Experiment (MSX)* mid-infrared data and *Infrared Astronomical Satellite (IRAS)* far-infrared data. Garay et al. (2004) noted strong 1.2-mm continuum emission from this source in the absence of emission in any of the *MSX* and *IRAS* bands. From the 1.2-mm dust continuum, along with the upper limits of *IRAS* fluxes, they inferred that the core is extremely cold (<17 K), massive and dense. Garay et al. (2004) hypothesized that the core is at an early stage of star formation, most likely before the development of an internal luminosity source, and will collapse to form high-mass star(s).

Pestalozzi, Humphreys & Booth (2002) conducted SIMBA 1.2-mm observations of the source based on the detection of a class II 6.6-GHz methanol maser from a survey by the Mt Pleasant Observatory (Ellingsen et al. 1996). Pestalozzi et al. (2002) suggested that there is a very deeply embedded object because of the detection of strong 1.2-mm emission and the methanol maser. Later, a class I 95.1-GHz methanol maser was detected by Ellingsen (2005) with the Mopra Telescope.

2 OBSERVATIONS AND DATA PROCESSING

The multi-molecular line data presented here were collected between 2004 July and 2006 October with the Mopra Telescope, operated by the Australia Telescope National Facility (ATNF). It has a full width to half-maximum (FWHM) beamsize of ∼32 arcsec at 100 GHz (Ladd et al. 2005). The observations were carried out with the new University of New South Wales (UNSW) Mopra Spectrometer (MOPS) digital filterbank backend and Monolithic Microwave Integrated Circuit (MMIC) receiver, except for ^{13}CO and C^{18}O which were observed with the Mopra Correlator (MPCOR) and the previous SIS receiver (Bains et al. 2006). According to Ladd et al. (2005) the main-beam efficiency at 86 GHz is 0.49, and at 115 GHz it is 0.42.

The observations are part of the on-going multi-molecular line survey (the 'Delta Quadrant Survey' or DQS) project carried out by UNSW, of the giant molecular cloud complex G333. The cold core G333.125−0.562 is part of the complex. The first paper featuring ^{13}CO is already published (Bains et al. 2006). In addition to the 3-mm multi-molecular line survey, NH$_3$ and H$_2$O (12 mm) maps of the core were also obtained during 2006 December with the Mopra Telescope. The main-beam efficiency for the 12-mm system is $\eta_{22\,\mathrm{GHz}} = 0.7$ and the FWHM beamsize is approximately 2 arcmin. The data presented in this work have a pointing accuracy of within ∼5 arcsec.

★E-mail: nlo@phys.unsw.edu.au

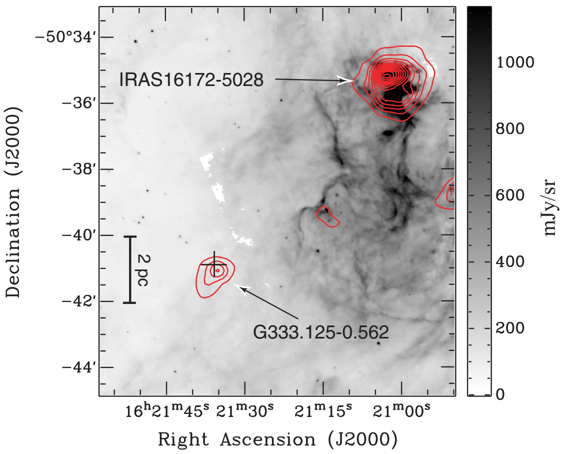

Figure 1. GLIMPSE 8-μm image (grey-scale) overlaid with the SIMBA 1.2-mm dust continuum (red contours). The contour levels start from 690 mJy beam^{-1} with increments of 690 mJy beam^{-1}. The arrows show the position of the core and the *IRAS* source, the cross shows the 6.7-GHz methanol maser, while the scale bar denotes 2 pc at a distance of 3.6 kpc. No 8-μm emission is evident at the position of the core.

3 RESULTS AND DISCUSSION

Shown in Fig. 1 is the *Spitzer* Galactic Legacy Infrared Midplane Survey Extraordinaire (GLIMPSE) 8-μm image (grey-scale) overlaid with the SIMBA 1.2-mm dust continuum (red contours) obtained from Mookerjea et al. (2004). From the image it can be seen that the core (bottom left) is isolated and has compact dust emission. No infrared emission is evident from it. Inspection of the *Spitzer* MIPSGAL images at 24 and 70 μm shows a source only at the longer wavelength. Thus this must be a cold dust core. From this core we have further detected emission from a number of molecular transitions: their observed parameters are summarized in Table 1. Among these, the detection of SiO ($J = 2{-}1$) is of particular interest. Presented in Fig. 2 is the integrated emission map of SiO (red contours) overlaid on CS (grey-scale); both maps have been smoothed to 36 arcsec. From the map we can see that there are two strong peaks of SiO emission: one is the luminous *IRAS* source IRAS 16172−5028 and the other one is from the cold dense core G333.125−0.562. This is quite different from the extended distribution seen in other molecular transitions in this region. Shown in the inset is the SiO velocity profile averaged over the core (dashed box); it is evident that the line profile is broad. We will first discuss the distribution of the molecules, followed by the physical properties derived for the core.

3.1 Distribution of the molecules

Presented in Fig. 3 are the integrated emission (zeroth moment) maps of the detected molecular lines over the velocity range of −80 to −40 km s^{-1}, except ^{13}CO and C^{18}O, which are integrated over the

Table 1. Summary of the observed and derived parameters of the molecular lines: centre velocity (V), line width (ΔV), peak brightness (T_{peak}), integrated brightness ($\int T_{\mathrm{MB}}\,\mathrm{d}v$), isotopic column density (N), virial mass (M_{vir}) and FWHM angular size (θ). The penultimate column is the abundance ratio (X) of the molecular line relative to H_2. For lines with more than one velocity component, parameters reported here are for the component associated with the core velocity, $-\,58\ km\ s^{-1}$. The uncertainty range is in parentheses.

Molecule	Transition	V (km s^{-1})	ΔV (km s^{-1})	T_{peak} (K)	$\int T_{\mathrm{MB}}\,\mathrm{d}v$ (K km s^{-1})	N (10^{14} cm^{-2})	M_{vir} (10^3 M$_{\odot}$)	θ (arcsec)	X (10^{-10})	Note
3-mm										
^{13}CO	1 – 0	−57.56 (0.03)	4.90 (0.06)	9.5	49.3 (0.8)	2.0×10^3	1.2	48	5.0×10^4	[ex]
C^{18}O	1 – 0	−56.63 (0.05)	5.1 (0.1)	2.6	14.1 (0.3)	5.2×10^3	1.3	48	1.3×10^4	[ex]
CS	2 – 1	−58.8 (0.3)	4.5 (0.7)	0.9	4.1 (1.3)	1.7	1.0	48	4.3	[ex]
C^{34}S	2 – 1	−57.7 (0.3)	3.1 (0.8)	0.3	1.0 (0.2)	0.6	0.5	54	1.5	[c]
HCO$^+$	1 – 0	−59.4 (0.1)	4.6 (0.1)	2.1	10.4 (0.4)	2.7	1.1	48	6.8	[ex]
HCN	1 – 0									[hf]
	F =2 − 1	−59.5 (0.1)	2.2 (0.3)	0.6	1.4 (0.2)	–	–	–	–	–
	F =0 − 1	−66.6 (0.1)	5.3 (0.4)	0.7	3.9 (0.3)	–	–	–	–	–
	F =1 − 1	−51.8 (0.4)	–	–	–	–	–	–	–	[I]
HNC	1 – 0	−59.07 (0.05)	3.9 (0.1)	2.2	9.2 (0.5)	$>3 \times 10^{-3}$	0.8	46	$>9 \times 10^{-3}$	[II]
N$_2$H$^+$	1 – 0	−58.8 (0.1)	4.0 (0.1)	1.0	3.9 (0.3)	24	3.3	99	61	[hf,c]
CH$_3$OH	$2_{02} - 1_{01}$ A$^+$	−58.0 (0.1)	4.2 (0.2)	1.2	5.2 (0.3)	–	–	84	–	[c,III]
HCCCN	11 – 10	−57.3 (0.2)	3.6 (0.5)	0.3	1.3 (0.2)	0.6	1.3	69	1.5	[c,IV]
HCCCN	10 – 9	−57.41 (0.09)	3.8 (0.2)	0.6	2.5 (0.1)	–	–	–	–	[c]
SO	$3_2 - 2_1$	−57.2 (0.2)	5.0 (0.5)	0.5	2.7 (0.2)	1.1	1.3	48	2.6	[II]
SiO	2 – 1 $v = 0$	−57.2 (0.3)	9.0 (1.0)	0.2	1.8 (0.2)	4.4	3.9	48	11	[II]
12-mm										
NH$_3$	(1,1)	−56.89 (0.02)	3.46 (0.03)	0.9	10.7 (0.2)	0.4	1.5	120	1	[hf,V]
NH$_3$	(2,2)	−57.2 (0.1)	3.7 (0.2)	0.4	2.7 (0.2)	–	–	–	–	[hf]
H$_2$O	$6_{16} - 5_{23}$	−53.9 (0.1)	2.0 (0.3)	0.1	0.24 (0.03)	–	–	–	–	[m]

Notes. [hf]: hyperfine structures; the peak brightness is for the main component, and the integrated brightness for the sum of all hyperfine components, except HCN, for which we list each hyperfine component; [m]: maser; [ex]: the molecular line emission is extended, hence we used the angular size of the dust continuum to derive the virial mass; [c]: compact emission; [el]: the emission is elongated; the angular size is the average of the RA and Dec.; [I]: the hyperfine component is blended with the −50 km s^{-1} velocity component; [II]: we derived the column density assuming that the line is optically thin, hence it and the abundance ratio are lower limits; [III]: no other CH$_3$OH transition detected, therefore column density cannot be calculated; [IV]: column density calculated using the rotational temperature (5.7 K) obtained from $J = 10{-}9$ and 11–10 lines; [V]: the beamsize at 22 GHz is ∼2 arcmin, therefore the source is unresolved; we took the angular size to be one beamwidth as there is no noticeable extended emission.

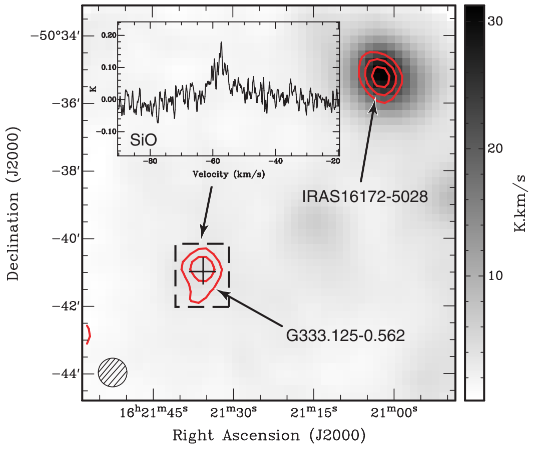

Figure 2. The integrated emission map of the SiO $J = 2{-}1$ transition (red contours) overlaid on the CS $J = 2{-}1$ transition (grey-scale). The contour levels start from 2.4 K km s^{-1} in steps of 0.8 K km s^{-1} (1σ), in terms of the main beam brightness temperature, T_{MB}. The cross shows the 6.7-GHz methanol maser; the hatched circle indicates the beam size. The inset is the velocity profile of SiO averaged over the region indicated by the dashed box. Note that the temperature scale of the SiO spectra is in antenna temperature.

ranges indicated in the figure. The molecular line emission peaks are coincident (within a beam) with the 1.2-mm dust, except for $C^{18}O$ which is offset by approximately 55 arcsec (∼1 pc at a distance of 3.6 kpc). Note that there is extended $C^{18}O$ emission towards the north of the dust peak. The low-density tracer CO is clearly more extended than the other molecules, which are sensitive to denser gas. Recent studies (Lintott et al. 2005) suggest that CS is a good tracer of dense cores in high-mass star-forming regions, in contrast to low-mass star formation where CS may be depleted. Since the peak matches well with the dust peak, this suggests that CS does not suffer from significant depletion. However, we do note that depletion could happen at smaller scales. Another feature evident in the HNC and HCO^+ maps is the tongue of extended emission to the south-west (arrow). A comparison between HCN and HNC integrated emission maps shows large differences in distribution, HCN being more extended than HNC, while at the same time the peak brightness of HCN is lower than that of HNC. Whether this is caused by optical depth effects needs further investigation. Although HCN and HNC have the same precursors ($HCNH^+$ and H_2CN^+) and similar dipole moments, it is believed that HCN is enhanced in warm environments in contrast to HNC, which forms preferentially in colder conditions (Kim et al. 2006). Hirota et al. (1998) found that the abundance ratio of [HNC]/[HCN] rapidly drops as the temperature exceeds a temperature of 24 K. N_2H^+ is known as a cold gas tracer as its abundance tends to be enhanced in cold dense cores, due to the depletion of CO, which decreases the destruction of N_2H^+ and H_3^+ (Womack, Ziurys & Wyckoff 1992; Hotzel, Harju & Walmsley 2004). Rather than reacting with CO to form HCO^+ and H_2, the H_3^+ ion reacts with N_2 to form N_2H^+. From the integrated emission map of N_2H^+, we see a compact distribution of N_2H^+. This suggests that the N_2H^+ is tracing the outer cold envelope of the dense core. The other two molecules that show a compact distribution are CH_3OH and HC_3N (both transitions), both of which trace dense gas. SiO and SO are known to be greatly enhanced in outflows and shocked regions (Martin-Pintado, Bachiller & Fuente 1992). Detecting both these species suggests that energetic activity associated with shock waves is present.

3.2 Physical properties

In order to derive the physical parameters, spectra were spatially averaged over the FWHM angular size for molecules with compact emission, otherwise over a 48-arcsec region, then fitted with a Gaussian in CLASS.[1] The fitted parameters, i.e. line width, centre velocity, brightness temperature and optical depth (from hyperfine structure fitting of N_2H^+ and NH_3), were then used to derive column densities and masses. The derived parameters are summarized in Table 1. The column densities were calculated with an excitation temperature of 15 K, which is the average of the dust and NH_3 values (see below). We note that the derived column densities vary by 20 per cent for the excitation temperature range (13–18 K). We have derived molecular abundances relative to the H_2 column density, which is obtained from the 1.2-mm dust continuum, $N_{H_2} \sim 4 \times 10^{23}$ cm^{-2}.

From the NH_3 $(J, K) = (1, 1)$ and (2,2) inversion transitions we have calculated the rotational temperature (T_{12}) of the core, following the method stated in Ungerechts, Winnewisser & Walmsley (1986). We assumed that *NH*$_3$ (1,1) and (2,2) are tracing the same volume of gas, and all hyperfine components have the same excitation temperature. With the above assumptions, we have derived the rotational temperature, $T_{12} = 13.1$ K, with an uncertainty range of 12.9–13.3 K. According to Danby et al. (1988), below 20 K the rotational temperature of NH_3 (1,1)–(2,2) matches the kinetic temperature (T_{kin}) well.

We are also able to determine a dust temperature, mass and luminosity from the spectral energy distribution (SED). Inspection of the GLIMPSE and MIPSGAL images of the core only shows evidence of emission at the longest wavelength (70 µm). Far-infrared balloon-borne measurements have been made at 150 and 210 µm by Karnik et al. (2001), through a 3-arcmin beam. Examination of the *Spitzer* infrared images shows that this emission must be confined to the G333.125−0.562 core. Hence we use the 150-µm, 210-µm and 1.2-mm fluxes to determine the SED, constraining the size by the angular size (48 arcsec) of the 1.2-mm core, and applying a greybody fit with a dust emissivity index of $\beta = 2$ (Hill et al. 2006). This yields the following parameters for the core: $T_{\mathrm{dust}} = 18.6 \pm 0.1$ K, $L_{\mathrm{bol}} = (8.5 \pm 0.3) \times 10^3\ \mathrm{L}_\odot$ and $M_{\mathrm{gas}} = 1.8 \times 10^3\ \mathrm{M}_\odot$. Taken with the angular size, these yield $\bar{n}_{H_2} \sim 1.3 \times 10^5$ cm^{-3} and $N_{H_2} \sim 4 \times 10^{23}$ cm^{-2}. We note that these parameters are similar to those derived by Garay et al. (2004) who made use of just the 1.2-mm flux, combined with upper limits at 60 and 100 µm from *IRAS* data – yielding an upper limit to the temperature of 17 K. Thus the dust-determined temperature is comparable to that derived from the NH_3 emission, giving us confidence in the conclusion that the core is exceedingly cold. If we assume that the molecular lines are thermalized then T_{kin} is approximately equal to the excitation temperature (T_{ex}) for each molecule.

Most of the detected molecular lines are peaked at ~ -57 km s^{-1}, except for HCO^+, HNC and N_2H^+ which are peaked at ~ -59 km s^{-1}. This likely due to lines being optically thick, for instance the $H^{13}CO^+$ line peaks at -57 km s^{-1}. The methanol maser also peaks at -57 km s^{-1}, with components at -53 and -63 km s^{-1} (Ellingsen 2005), indicative of outflows. The water maser is at -54 km s^{-1}. The line widths for most of the molecules are between 3 and 5 km s^{-1} as opposed to the ∼0.5 km s^{-1} predicted for quiescent gas dominated by thermal broadening, suggesting that the core is turbulent. The SiO, however, has the largest line width amongst

---

[1] Part of the GILDAS software package by IRAM (http://www.iram.fr/IRAMFR/GILDAS/).

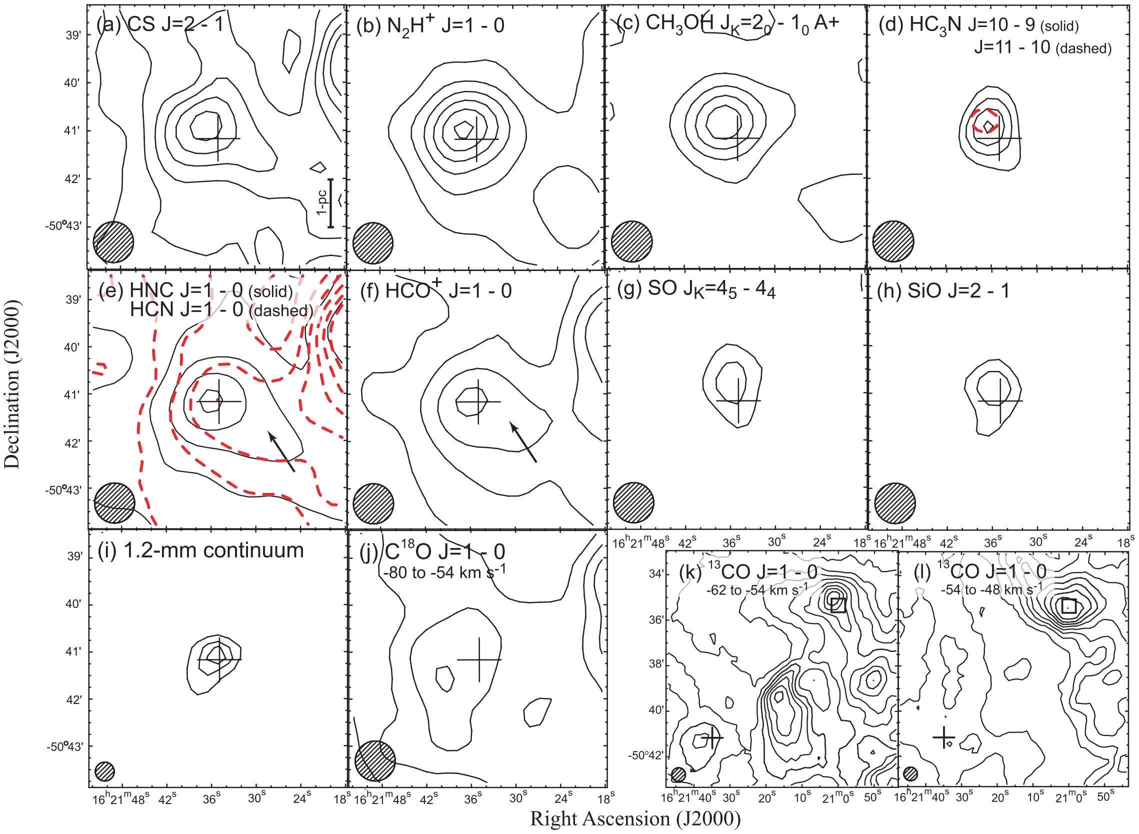

Figure 3. (a) to (j) Integrated emission maps of various molecular lines, as indicated for the core G333.125−0.562. The contour levels start from 3σ of the rms. The contour levels are in steps of 3σ for N_2H^+, CH_3OH, HNC, HCN, HCO^+, $C^{18}O$ and 1.2-mm continuum, and in steps of 1σ for CS, HC_3N (both transitions), SO and SiO. The rms is 1.1 K km s^{-1} for CS and CH_3OH, 0.91 K km s^{-1} for N_2H^+, HC_3N ($J = 11$–10) and SO, 0.82 K km s^{-1} for HNC, HCO^+ and SiO, 0.61 K km s^{-1} for HC_3N ($J = 10$−9) and HCN, and 1.2 K km s^{-1} for $C^{18}O$. The temperatures are in $T^*_{\rm MB}$. The integrated velocity range is from −80 to −40 km s^{-1}, except $C^{18}O$ which is from −80 to −54 km s^{-1}. The arrows show the tongue of extended emission in the south-west direction. (k)^{13}CO integrated emission map from −62 to −54 km s^{-1}, over a region covering the core (lower left) and IRAS 16172−5028 (upper right). (l) Same as (k) but over the velocity range −54 to −48 km s^{-1}. Contour levels for the ^{13}CO maps start from 20 per cent of the peak, in increments of 10 per cent. The cross marks the peak of the 1.2-mm continuum and the square is the ultracompact H II region associated with IRAS 16172−5028. The beam sizes are indicated with the hatched circles; the scale bar in panel (a) denotes 1 pc at a distance of 3.6 kpc.

the detected molecular lines, 9.0 ± 1.1 km s^{-1}, lending further support to being associated with an outflow. Its abundance with respect to H_2 has an upper limit of $\sim 10^{-12}$ in quiescent gas, but is greatly enhanced in powerful shocks, up to $\sim 10^{-7}$ (e.g. Ziurys, Friberg & Irvine 1989; Martin-Pintado et al. 1992). We have determined the abundance to be $\sim 10^{-9}$, in between these extremes. A similar abundance ratio has been found in molecular outflows (e.g. Codella, Bachiller & Reipurth 1999; Garay et al. 2002). A follow-up CO ($J = 1 - 0$) molecular line observation over a 5 × 5-arcmin^2 region of the core was taken in 2007 June: the spectra clearly show line wings; however, they are confused with multiple velocity components and need further investigation.

4 WHAT IS GENERATING THE SIO EMISSION: OUTFLOWS OR COLLISIONS?

The optically thick isotopomers clearly show two different velocity components, indicating that there are two separate clouds in this region. The cloud at ∼ −50 km s^{-1} is associated with IRAS 16172−5028, and is at the ambient velocity of the G333 giant molecular cloud (see Fig. 3l). The other cloud at ∼ −58 km s^{-1} is associated with the cold core G333.125−0.562 (Fig. 3k). The SiO emission could be generated by these two clouds colliding, but we consider this unlikely. First, consider the confined emission of the SiO, localized to the dust core itself. If it were due to a cloud–cloud collision we would expect a more extended distribution. Secondly, for a cloud–cloud collision there should be distinctive features in the density structure. Shown in Fig. 4 is the ^{13}CO integrated emission map of velocity range −52 to −50 km s^{-1}. Note the sharp edge (arrow) on the left-hand side of the *IRAS* source (square), suggesting compression of the gas here. However, no compression is evident associated with the cold core (cross) at the velocity observed.

5 SUMMARY AND CONCLUSION

From our molecular line survey of the G333 giant molecular cloud, we have detected thermal SiO emission from the massive cold dense core G333.125−0.562, with an abundance enhanced over typical unshocked molecular cloud values. This core has a gas mass of 1.8×10^3 M$_\odot$, is undetected up to 70 μm and has compact 1.2-mm dust continuum emission. From the NH_3 inversion lines we have derived a temperature of 13 K, which is comparable to that derived from the SED (19 K). The detection of compact emission from a cold gas tracer (N_2H^+) suggests that this is a dense cold core. Typical

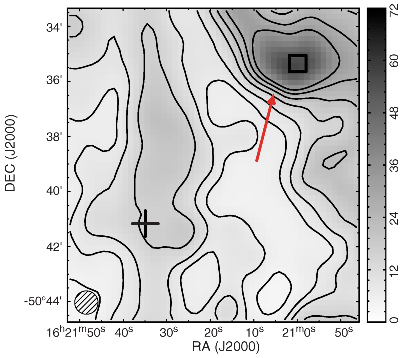

Figure 4. The integrated emission map of ^{13}CO ($J = 1{-}0$) from -52 to -50 km s^{-1}. The contour levels are 1.4, 4.3, 7.1, 10, 21, 27 and 33 K km s^{-1}. The temperature is in terms of the main beam brightness temperature. The cross marks the cold core G333.125−0.562 and the square marks IRAS 16172−5028. The arrow indicates a likely region where the gas is being compressed.

line widths are between 4 and 5 km s^{-1}, indicating that the core is turbulent, as expected in massive star formation.

In conclusion, from these observations we believe that the cold massive core harbours a deeply embedded, massive protostellar object that is driving an outflow. This is occurring at a very early stage of star formation, prior to the creation of an infrared source in the core.

ACKNOWLEDGMENTS

The Mopra Telescope is part of the Australia Telescope and is funded by the Commonwealth of Australia for operation as National Facility managed by CSIRO. The University of New South Wales Digital Filter Bank used for the observations with the Mopra Telescope was provided with support from the Australian Research Council. We thank the reviewer for constructive comments which improved this Letter, T. Wong for his work on C^{18}O data, and S. N. Longmore for help in analysing the NH$_3$ data. This research (GLIMPSE and MIPSGAL images) has made use of the NASA/IPAC Infrared Science Archive which is operated by the Jet Propulsion Laboratory, California Institute of Technology, under contract with NASA.

REFERENCES

Bains I. et al., 2006, MNRAS, 367, 1609
Codella C., Bachiller R., Reipurth B., 1999, A&A, 343, 585
Danby G., Flower D. R., Valiron P., Schilke P., Walmsley C. M., 1988, MNRAS, 235, 229
Ellingsen S. P., 2005, MNRAS, 359, 1498
Ellingsen S. P., von Bibra M. L., McCulloch P. M., Norris R. P., Deshpande A. A., Phillips C. J., 1996, MNRAS, 280, 378
Faúndez S., Bronfman L., Garay G., Chini R., Nyman L.-Å., May J., 2004, A&A, 426, 97
Garay G., Mardones D., Rodríguez L. F., Caselli P., Bourke T. L., 2002, ApJ, 567, 980
Garay G., Faúndez S., Mardones D., Bronfman L., Chini R., Nyman L.-Å., 2004, ApJ, 610, 313
Hill T., Thompson M. A., Burton M. G., Walsh A. J., Minier V., Cunningham M. R., Pierce-Price D., 2006, MNRAS, 368, 1223
Hirota T., Yamamoto S., Mikami H., Ohishi M., 1998, ApJ, 503, 717
Hotzel S., Harju J., Walmsley C. M., 2004, A&A, 415, 1065
Karnik A. D., Ghosh S. K., Rengarajan T. N., Verma R. P., 2001, MNRAS, 326, 293
Kim S.-J., Kim H.-D., Lee Y., Minh Y. C., Balasubramanyam R., Burton M. G., Millar T. J., Lee D.-W., 2006, ApJS, 162, 161
Ladd N., Purcell C., Wong T., Robertson S., 2005, Publ. Astron. Soc. Aust., 22, 62
Lintott C. J., Viti S., Rawlings J. M. C., Williams D. A., Hartquist T. W., Caselli P., Zinchenko I., Myers P., 2005, ApJ, 620, 795
Lovas F. J., Johnson D. R., Snyder L. E., 1979, ApJS, 41, 451
Martin-Pintado J., Bachiller R., Fuente A., 1992, A&A, 254, 315
Mookerjea B., Kramer C., Nielbock M., Nyman L.-Å., 2004, A&A, 426, 119
Pestalozzi M., Humphreys E. M. L., Booth R. S., 2002, A&A, 384, L15
Ungerechts H., Winnewisser G., Walmsley C. M., 1986, A&A, 157, 207
Womack M., Ziurys L. M., Wyckoff S., 1992, ApJ, 387, 417
Ziurys L. M., Friberg P., Irvine W. M., 1989, ApJ, 343, 201

This paper has been typeset from a TEX/LATEX file prepared by the author.